PNAS
www.pnas.org

Supplementary Information for

Cell Membrane Camouflaged Liposomes for Tumor Cell-Selective Glycans Engineering and Imaging in vivo

Zhengwei Liu[a,b,1], Faming Wang[a,b,1], Xinping Liu[a,c], Yanjuan Sang[a,c], Lu Zhang[a,b], Jinsong Ren[a,c], and Xiaogang Qu*[a,c]

*Xiaogang Qu

Email: xqu@ciac.ac.cn

This PDF file includes:

Supplementary text

Figures S1 to S41, Table S1

SI References

Supplementary Information Text

Materials and Methods

1. Reagents and materials

DSPE-PEG-NH_2, DSPE-PEG-folate, methyl-β-cyclodextrin (MBD), chlorpromazine (CHL) and amiloride (AMI) were purchased from Aladdin. DOPE, Ac_4ManNAz, Ac_4GalNAz and DBCO-Cy5 were provided by Sigma-Aldrich. Phosphine-PEG_3-biotin was from Cayman. Membrane protein extraction kit and phenylmethanesulfonyl fluoride (PMSF) were provided by Beyotime Institute of Biotechnology (China). Ultrapure water (18.2 MΩ; Millpore Co. USA) was used throughout the experiment.

2. Apparatus and characterization

UV-Vis absorbance measurement was carried out on a JASCO V-550 UV-Vis spectrophotometer. Fluorescence spectra were detected by JASCO F-6000 fluorescence spectrometer with a Peltier temperature control accessory. An Olympus BX-51 optical equipped with a CCD camera was used for capturing fluorescence images. The ζ-potential and DLS size of the nanoparticles in water was obtained on a Zetasizer 3000HS analyzer. Transmission electron microscopic (TEM) images of cells were captured with a FEI TECNAI G2 20 high-resolution transmission electron microscope operating at 200 kV. The flow cytometry data was obtained by BD LSRFortessa™ Cell Analyzer. The CLSM images were acquired using a (Nikon Eclipse Ni-E, Japan) top-of-the-line motorized upright confocal laser scanning microscopy.

3. Protein characterization of GL@cM

Protein characterization was conducted using sodium dodecyl sulfate-polyacrylamide gel electrophoresis (SDS-PAGE) method reported in literature (1). 10 μL of the GL@cM , cM and GL samples were loaded into each well of SDS-PAGE gel. Protein staining was accomplished using Coomassie Blue and destained in water overnight before imaging. For western blotting analysis, protein was transferred to Protran nitrocellulose membranes (Millipore) using an XCell II Blot Module (Tanon) in transfer buffer. Membranes were probed using antibodies against N-cadherin (Abcam), CD-47 (Abcam), and galectin-3 (Abcam) along with either horseradish peroxidase (HRP)-conjugated anti-rabbit IgG (Bioss). Films were developed using ECL western blotting substrate (BestBio) and developed with the Tanon 4800 Automatic Chemiluminescence Image Analysis System.

4. pH-responsive ability of liposome

To determine the pH-sensitive characteristic of this liposome, Rhodamine B (denoted as RB, 2mg) was specifically chosen as the Ac_4GalNAz substitute encapsulated by liposome (RB-L) as previous method, loading ratio of which was 15.6%. The RB release experiments were divided into two groups: (1) pH 7.4; (2) pH 5.0 phosphate buffered saline (PBS 10 mM). RB-L (1 mg mL^{-1}, 5 mL) was dispersed into 5 mL PBS at different pH under stirring at 37 °C in the capped vials. At predetermined time intervals, 200 μL of the buffer solution was removed and

the supernatant was used for UV-vis spectrum measurement of RB. The cumulative amounts of RB released were determined according to the UV-vis absorption intensity at 552 nm, using the standard calibration curve.

5. Measurement of protein adsorption

GL and GL@cM nanoparticles of defined amount were incubated with 1 mg mL^{-1} fluorescent IgG solution under continuous mixing on a shaker for 2 hours. Nanoparticles were collected by centrifugation and washed with PBS for 3 times, and then redispersed in 0.5 mL PBS. The fluorescence spectra and intensity of the nanoparticles suspension were recorded by JASCO F-6000 fluorescence spectrometer.

The serum stability of the prepared GL@cM and GL were carried out. Specifcally, defined amount of GL@cM and GL were incubated with 50% Fetal Bovine Serum at 37 °C for 12h. Nanoparticles were collected by centrifugation and washed with PBS for 3 times, then the size change were measured.

6. Cell culture

RAW 264.7 mouse leukemia cells of monocyte macrophage cells, MCF-7 human breast cancer cells, Hela human cervical carcinoma cells, A549 human non small cell lung cancer cell, CT26 mouse colon cancer cells, 4T1 mouse breast cancer cells, B16-F10 mouse melanoma cells were cultured in DMEM containing 10% FBS, 100 units/ml Penicillin G and 100 μg/ml streptomycin at 37 °C in 5% CO_2 humidified air unless otherwise noted. MDA-MB-436 and MDA-MB-231 triple-negative breast cancer cells were cultured in L15 containing 10% FBS, 100 units/ml Penicillin G and 100 μg/ml streptomycin at 37 °C.

7. In vitro evaluation of phagocytosis

Phagocytosis was evaluated by analyzing the nanoparticles uptake by the murine macrophage cell line RAW 264.7. RAW264.7 cells were planted in 24-well plates at the density of 5×10^5 per well and allowed to adhere for 24 h, respectively. After that, RB-L (30 μg mL^{-1}, RB~4.6 μg/mL), RB-L@HeLa and RB-L@MCF-7 (with the same concentration of RB determined by UV-vis spectrum) were added and incubated with the cells for 4 h. And then, the cells were washed with PBS for 3 times, stained by Hoechst 33342 for 15 min before fluorescence analysis (images were obtained using the confocal laser scanning microscopy). Furthermore, the cellular uptake of RB-L, RB-L@HeLa and RB-L@MCF-7 against RAW264.7 cells was also measured by flow cytometry analysis.

8. In vitro evaluation of tumor targeting of RB-L@cM to homotypic cells

Confocal laser scanning microscopy (CLSM) and flow cytometric assay were employed to investigate the homotypic targeting effect of RB-L coated with HeLa and MCF-7 cell membranes. For CLSM observation, HeLa, MCF-7, A549, 4T1, and CT26 cells were seeded in 24-well plates at a density of 5×10^5 cells and incubated at 37 ºC for 24 h. Then, the medium

was replaced with the fresh medium containing RB-L@HeLa or RB-L@ MCF-7 (RB~4.5 μg/mL). After 4 h co-incubation, the medium was removed and the cells were washed several times with PBS. After further incubation of Hoechst 33342 solution for 15 min at 37 ºC, the cells were photographed by CLSM.

Furthermore, the cellular targeting of RB-L@HeLa or RB-L@ MCF-7 towars HeLa, MCF-7, A549, 4T1, and CT26 cells were also measured by flow cytometry. The mean intensity of blank HeLa, MCF-7, A549, 4T1, and CT26 cells was chosen as control.

9. The metabolic incorporation of Ac_4GalNAz in vitro

HeLa and MCF-7 cells were seeded in 24-well plates for fluorescence microscopy analysis and flow cytometry experiments, cultured for 24 h. Then, the medium was replaced with the fresh medium containing GL@FA, GL@HeLa or GL@MCF-7 for 24 h at concentrations indicated (calculated based on Ac_4GalNAz) (2). After metabolic incorporation, the cells were washed three times with PBS containing 1% FBS, followed by incubation for 30 min in PBS containing 0.5% FBS and 50 μM DBCO-Cy5. The cells were washed three times with PBS to remove excess DBCO-Cy5. For confocal fluorescence microcopy, the cells were stained for 10 min with 10 μg mL^{-1} Hoechst 33342. The cells were then washed three times and imaged with confocal fluorescence microscope.

10. Western blotting analysis of cells treated with GL@cM.

HeLa cells were pretreated with GL@FA (50 μM of Ac_4GalNAz), GL@HeLa (50 μM of Ac_4GalNAz) or blank DMEM as control for 24 h and washed with PBS (pH 7.4) twice, then harvested from the plates and centrifuged at 1800 rpm for 3 min. Cells were re-suspended and incubated in 100 μL of lysis buffer containing protease inhibitor PMSF at 4 °C for 30 min and centrifuged for 20 min at 11000 rpm to get supernatant solution. The solution lysate (5 mg/mL, 50 μL) were incubated with phosphine-PEG3-biotin (5 μL, 5 mM in DPBS) for 6 h at 37 °C (3). Then the samples were resolved by 10% SDS/PAGE and transferred to nitrocellulose membranes (Millipore) using an XCell II Blot Module (Tanon) in transfer buffer. The membranes were blocked in 5% non-fat milk for 1.5 h. Then, the membrane was incubated with streptavidin-HRP (diluted 1:2000 in TBST) overnight at 4 °C. The membrane was developed by using ECL Western Blotting Substrate.

11. Internalization and intracellular release mechanism of EMP nanoparticles

To determine the endocytosis pathways, HeLa cells were incubated with RB-L@HeLa nanoparticles and several inhibitors for 2 hours (4). More specifically, chlorpromazine (CHL, inhibitor of clathrin-mediated endocytosis, 10 μg mL^{-1}), amiloride (AMI, inhibitor of Na+/H+ pump related macropinocytosis, 100 μg mL^{-1}) and methyl-beta cyclodextrin (MBD, inhibitor of cholesterol-dependent endocytosis, 5 mM) were used. After incubation, cells were washed, detached, and analyzed by the flow cytometry for quantification.

For intracellular trafficking of internalization of RB-L@HeLa nanoparticle by HeLa tumor cells, RB-L@HeLa (RB~4.5 μg/mL) were added to cultured HeLa cells. Cells were incubated at 37 °C and 5% of CO_2 for 1, 2, 4 and 8 hours, respectively. At the end of each incubation, the medium was removed, and the cells were washed with PBS 3 times. Then, the cells were washed by PBS for 3 times and stained with LysoTracker Green for 30 min and Hoechst 33342 for 15 min, respectively. The samples were analyzed by a Laser scanning confocal microscope. As for intracellular colocalization of RB-L@HeLa with endosome, cells were incubated with RB-L@HeLa (RB~4.5 μg/mL) for 1, 2, 4 and 8 hours, respectively. After fixing with 4% PFA for 10 min and permeabilizing with 0.1% Triton X-100 for 10 min, the cells were blocked with 5% BSA for 30 min and stained with 5 μg/mL rabbit anti-ENTR1 (Sangon Biotech) in 1% BSA at RT for 1 h (5). The cells were then stained with 5 μg/mL anti-rabbit IgG-FITC (Sangon Biotech) at RT for 1 h. After staining the nuclei with 10 μg/mL Hoechst 33342 for 10 min, the cells were subjected to confocal fluorescence imaging

12. Animal experiments

Female Balb/c nude mice and Balb/c mice of 16 g body-weight were purchased from Medical Experimental Animal Center of Jilin University (Changchun, China), and kept under SPF condition with free access to standard food and water.

12.1. Plasma pharmacokinetics

RB-L@HeLa and RB-L nanoparticles (10 mg kg^{-1}) were intravenously administered to healthy mice. For fluorescence imaging visualization, 30 μL blood samples were repeatedly collected by tail snip before treatment and at 10min, 0.5, 1, 2, 4, 6, 8, 12 h post-injection and analyzed using a Maestro in vivo fluorescent imaging system (Cambridge Research & Instrumentation Inc., Woburn, USA) to detect the fluorescent signal (550 nm excitation/575 nm emission). For plasma florescence quantification, after administration for different time periods (10min, 0.5, 1, 2, 4, 6, 8, 12, and 24 h), the mice were anesthetized and blood samples were collected. The plasma was obtained by centrifugation at 1000g for 10 min and used for florescence detection by a fluorescence spectrophotometer.

12.2. Tumor model and nanomaterials administration

For tumor targeting experiments, mouse tumors were established by subcutaneous injection of HeLa (2×10^7 cells/0.1 mL/ left flank) and MCF-7 (1×10^7 cells/0.1 mL/ right flank) in both flanks of each nude mouse. Five days later, the mice were randomly assigned to 4 groups (n=3 per experimental group). Tumor volume (V) was estimated from caliper measurements of tumor length (l) and width (w), and assuming the volume $V=(\pi/6) \times l \times w^2$. Tumor growth was monitored daily until it reached the acceptable size. When tumors reached 8-10 mm in diameter, mice were injected i.p. daily with Ac_4GalNAz (60mg/kg) or i.v. daily with GL@HeLa, GL@MCF-7, and GL (60mg/kg, calculated based on Ac_4GalNAz) for four consecutive days. On the fifth day, the mice were analyzed with in vivo and ex vivo fluorescence imaging.

12.3. In vivo and ex vivo fluorescence imaging

After the administration of Ac_4GalNAz, GL@cM, and GL, the mice were injected with DBCO-Cy5 (2mg/kg) at the tail vein and allowed to react with the metabolized azidosugars. Animals were then euthanized and imaged by the Maestro in vivo fluorescent imaging system (Cambridge Research & Instrumentation Inc., Woburn, USA). Excitation and emission spots were faster-scanned in 1 mm steps to generate emission wavelength scans. A 670 nm pulsed laser diode was used to excite Cy5 molecules. Fluorescence emission at 700 nm was collected and detected with a fast photomultiplier tube and a time-correlated single photon counting system. The in vivo fluorescence images were quantified by measuring NIRF signal intensity at the region of interest (ROI) using Caliper Living image® software. The mean fluorescence was normalized. All values were expressed as means ± s.d. for groups of at least three animals.

For ex vivo imaging, animals were euthanized, the major tissues and tumors were dissected from mice 6 h post-injection of DBCO-Cy5 before whole-body hemoperfusion to exclude the blood chromophore interference.

12.4. Imaging of tumor tissue sections

The DBCO-Cy5 treated mouse tumors were dissected and fixed in 4 % (v/v) buffered formalin solution, and frozen in optimum cutting temperature (OCT) compound on dry ice, and stored at -80 °C until use. Sections were cut on a cryostat (10 μm in thickness) and picked up on slides with poly-D-lysine, dried at 45 °C, protected from light. The tissue sections were imaged using a CLSM.

13 Breast cancer subtypes model.

For breast cancer subtypes targeting experiments in vitro, MDA-MB-436, MDA-MB-231 and MCF-7 cells were seeded in 24-well plates for fluorescence microscopy analysis, cultured for 24 h. Then, the medium was replaced with the fresh medium containing ML@MDA-436, ML@MDA-231 and ML@MCF-7 (50 μM, calculated based on Ac_4GalNAz) for 24 h. After metabolic incorporation, the cells were washed three times with PBS containing 1% FBS, followed by incubation for 30 min in PBS containing 0.5% FBS and 50 μM DBCO-Cy5. The cells were washed three times with PBS to remove excess DBCO-Cy5. For fluorescence microcopy, the cells were stained for 10 min with 10 μg mL^{-1} Hoechst 33342. The cells were then washed three times and imaged with fluorescence microscope.

For in vivo experiments, mouse tumors were established by subcutaneous injection of MDA-MB-436 (1×10^7 cells/0.1 mL/ left flank) and MCF-7 (1×10^7 cells/0.1 mL/ right flank) in both flanks of each nude mouse. Five days later, the mice were randomly assigned to 3 groups (n=5 per experimental group). Tumor growth was monitored daily until it reached the acceptable size. When tumors reached 8-10 mm in diameter, mice were injected i.v. daily with ML@MDA-436, ML@MCF-7, and ML@FA (60mg/kg, calculated based on Ac_4ManNAz) for

four consecutive days. On the fifth day, the mice were injected with DBCO-Cy5 (2mg/kg) at the tail vein and allowed to react with the metabolized azidosugars. Animals were then imaged by the Tanon in vivo fluorescent imaging system. The in vivo fluorescence images were quantified by measuring NIRF signal intensity at the region of interest (ROI) using Tanon InVivo analysis software.

14 The 4T1 orthotopic mammary tumor spontaneous metastasis model of BALB/c mice.

5×10^6 4T1 cells were subcutaneously injected into the left mammary gland of immune competent mice to initiate the 4T1 orthotropic metastasis tumor model. Five days later, the mice were randomly assigned to 3 groups (n=5 per experimental group). After tumor growth for 6, 16, and 26 days, the mice were administered with GL@4T1 (60mg/kg, calculated based on Ac_4GalNAz) with the same dosages for another 4 days, followed by injection with DBCO-Cy5 for in vivo and ex vivo imaging on day 10, 20, and 30, respectively. The lung tissues and metastatic nodules were imaged. Hematoxylin and eosin (H&E) were applied to detect the micro-metastasis lesions on the lungs.

15 Western blot analysis of tumor tissues.

After tumor growth for 6, 16, and 26 days, 4T1 tumor bearing mice were intravenously injected with GL@4T1 (60 mg kg^{-1} of Ac_4GalNAz) once a day for 4 days. The mice were sacrificed at 10, 20, and 30 days, and the tumors were dissected, incubated with 500 μL lysis buffer (1% SDS, 100 mM Tris·HCl, pH 7.4) containing protease inhibitor cocktail at 4 °C for 30 min, and removed insoluble debris by centrifugation for 20 min at 11000 rpm. Then, Western blot analysis was performed with phosphine-PEG_3-biotin by the same method as the cell lysate analysis.

16 Tumor-derived cell membrane for homotypic-targeted metabolic glycan labeling

4T1 and B16F10 tumor cell was isolated from 4T1 and B16F10 tumor tissue acquired by surgical operation and cultured for further membrane extraction (6, 7). After membrane extraction, the GL@4T1 and GL@B16 were prepared as before for in vitro and in vivo metabolic glycan labeling.

For in vitro experiment, 4T1 cells were seeded in 24-well plates for fluorescence microscopy analysis, cultured for 24 h. Then, the medium was replaced with the fresh medium containing GL@4T1 (50 μM, calculated based on Ac_4GalNAz) for 24 h. After metabolic incorporation, the cells were washed three times with PBS containing 1% FBS, followed by incubation for 30 min in PBS containing 0.5% FBS and 50 μM DBCO-Cy5. The cells were washed three times with PBS to remove excess DBCO-Cy5. For fluorescence microcopy, the cells were stained for 10 min with 10 μg mL^{-1} Hoechst 33342. The cells were then washed three times and imaged with fluorescence microscope.

For in vivo experiment, mouse tumors were established by subcutaneous injection of 4T1 (5×10^6 cells/0.1 mL/ left flank) and B16F10 (5×10^6 cells/0.1 mL/ right flank) in both flanks of

each nude mouse. Five days later, the mice were randomly assigned to 4 groups (n=5 per experimental group). Tumor growth was monitored daily until it reached the acceptable size. When tumors reached 8-10 mm in diameter, mice were injected i.v. daily with GL@4T1, GL@B16, GL@FA, and GL (60mg/kg, calculated based on Ac_4GalNAz) for four consecutive days. On the fifth day, the mice were injected with DBCO-Cy5 (2mg/kg) at the tail vein and allowed to react with the metabolized azidosugars. Animals were then imaged by the Tanon in vivo fluorescent imaging system. The in vivo fluorescence images were quantified by measuring NIRF signal intensity at the region of interest (ROI) using Tanon InVivo analysis software.

To study the differences of metabolic glycan labeling specificity between GL@4T1-au and GL@4T1-al, 4T1 tumor derived cells were treated with GL@4T1-au and GL@4T1-al (50 μM, calculated based on Ac_4GalNAz) for 24 h. After metabolic incorporation, the cells were washed three times with PBS containing 1% FBS, followed by incubation for 30 min in PBS containing 0.5% FBS and 50 μM DBCO-Cy5. The cells were washed three times with PBS to remove excess DBCO-Cy5. For fluorescence microcopy, the cells were stained for 10 min with 10 μg mL^{-1} Hoechst 33342. The cells were then washed three times and imaged with fluorescence microscope. In addition, 4T1 tumor-bearing mice were injected with GL@4T1-au and GL@4T1-al (60mg/kg, calculated based on Ac_4GalNAz) for four consecutive days. On the fifth day, the mice were injected with DBCO-Cy5 (2mg/kg) at the tail vein and allowed to react with the metabolized azidosugars. Animals were then imaged by the Tanon in vivo fluorescent imaging system. The in vivo fluorescence images were quantified by measuring NIRF signal intensity at the region of interest (ROI) using Tanon InVivo analysis software.

17 Statistical analysis

Intensity of fluorescence microscopy images was measured by ImageJ software. Fluorescence intensity of confocal microscopy images were measured by Nikon Eclipse Analysis software. In Figure 5, the whole-body fluorescence images were captured and analyzed by Maestro in vivo fluorescent imaging system and Caliper Living image® software. In Figure 6, S32, S34, S39 and S41, the whole-body and organs fluorescence images were captured and analyzed by Tanon in vivo fluorescent imaging system and Tanon InVivo analysis software. All data were expressed in this article as mean result ± standard deviation (s.d.). All figures shown in this article were obtained from three independent experiments with similar results unless specific mention. The statistical analysis was performed by using Origin 8.0 software. Statistical evaluation was performed using unparied Student's two-sided t test analysis. Asterisks indicate significant differences (NSD: no significant difference,*$P < 0.01$, **$P < 0.005$, ***$P < 0.001$).

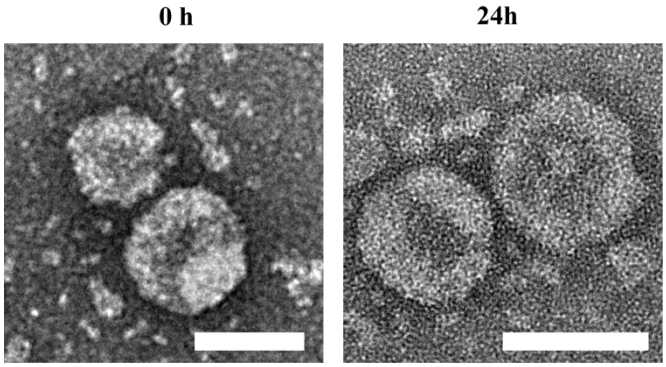

Figure S1. The TEM morphological change of GL with time when incubated in PBS at pH 7.4. Scale bar: 100 nm.

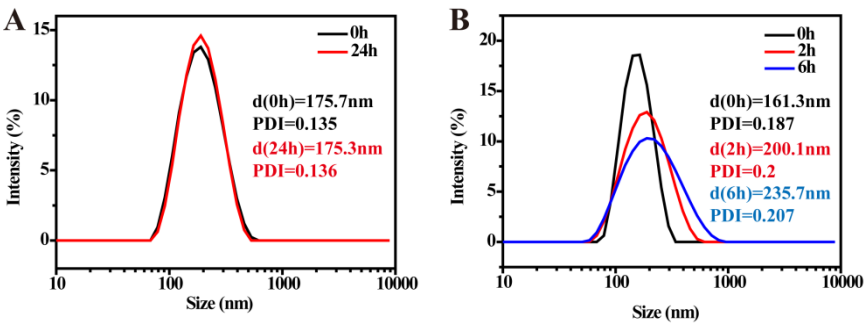

Figure S2. The pH-responsive size changes of GL with time. (A) Size changes in PBS at pH 7.4. (B) Size changes in PBS at pH 5.0.

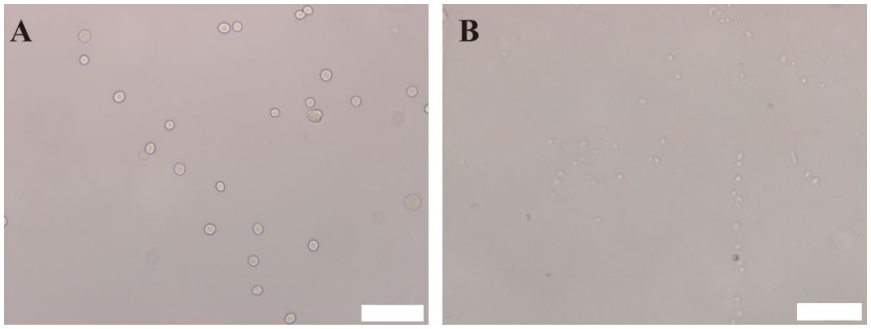

Figure S3. (A) The images of intact cells. Scale bar: 100 μm. (B) The images of cell membranes debris. Scale bar: 50 μm. They were observed by optical microscopy.

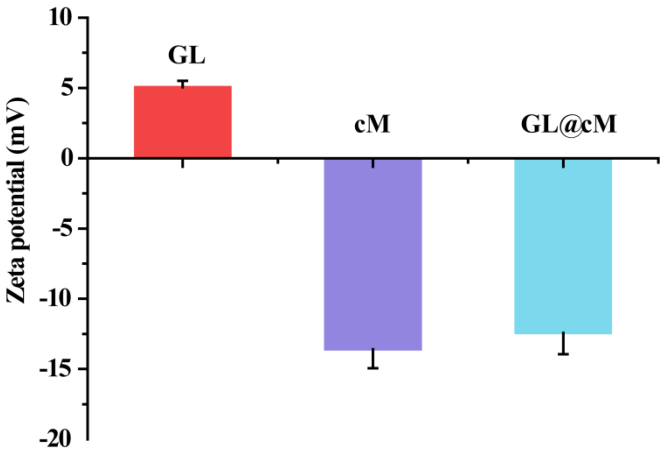

Figure S4. Zeta potential of GL, cM, and GL@cM nanoparticles.

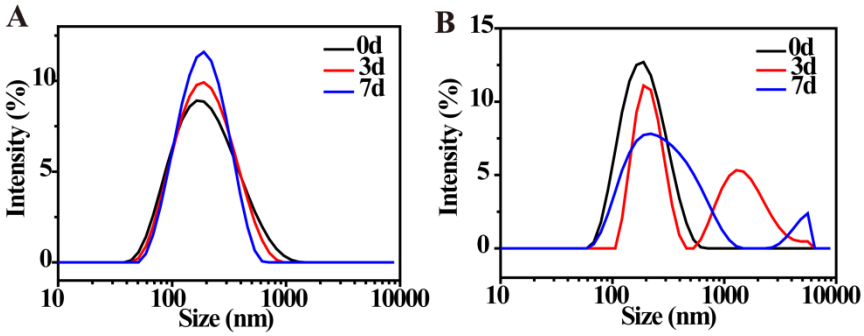

Figure S5. The stability of GL@cM with time in PBS at pH 7.4. (A) DLS size distribution of GL@cM in pH 7.4 PBS. (B) DLS size distribution of GL in pH 7.4 PBS.

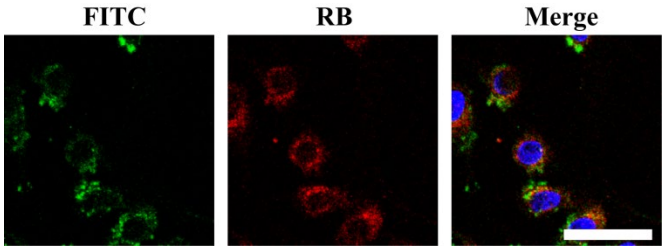

Figure S6. Colocalization of liposomes and cancer cell membranes in cell. The green fluorescence was from the membrane labeled with FITC, the red fluorescence was from encapsulated RB in liposomes. The nuclei were stained by Hoechst 33342. Scale bar: 50 μm.

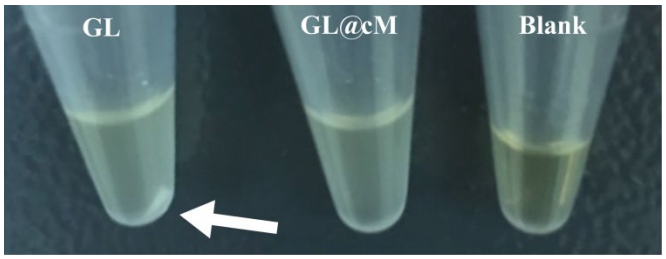

Figure S7. The digital picture showed the good stability of GL@cM in 50% FBS over 12h. The bare GL would aggregate and give precipitates due to the protein adsorption.

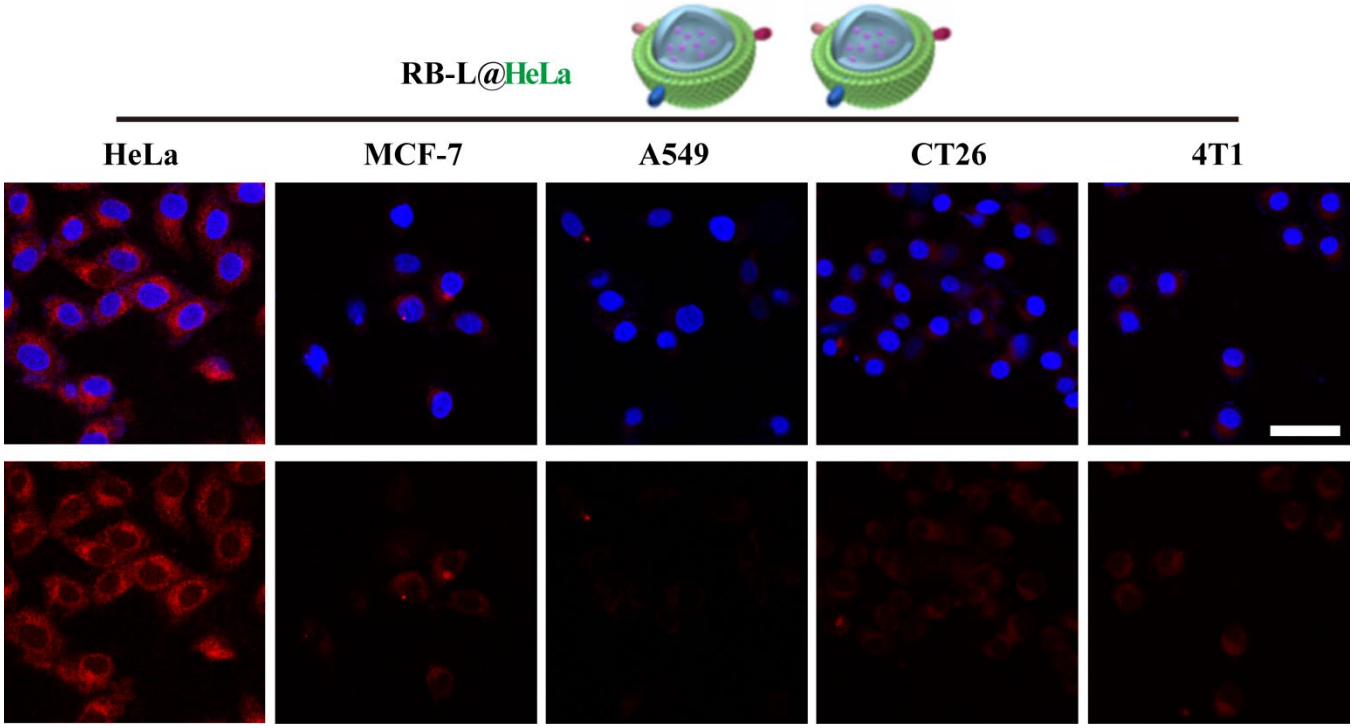

Figure S8. CLSM images of five cell lines including HeLa, MCF-7, A549, CT26 and 4T1 cells upon 4 h incubation with RB-L@HeLa. The nuclei were stained with Hoechst (blue). Scale bar: 50 μm.

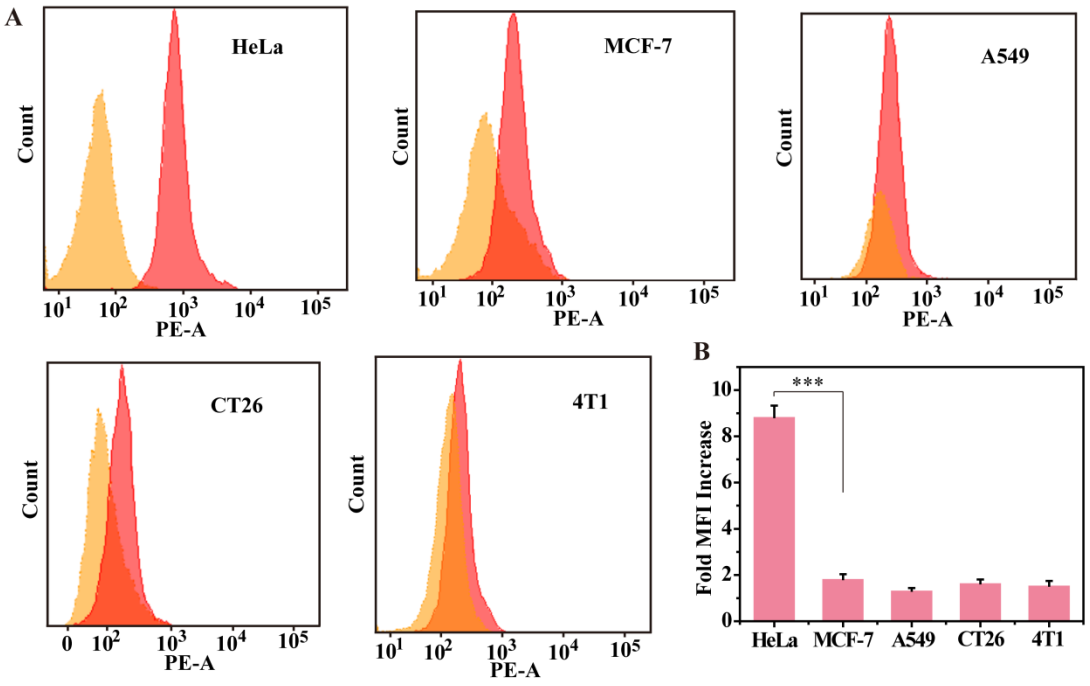

Figure S9. (A, B) Flow cytometry analysis of various cells incubated with RB-L@HeLa for 4 h. Error bars were calculated on the basis of three independent experiments. Asterisks indicated significant differences (*P < 0.05, **P < 0.01, ***P < 0.001).

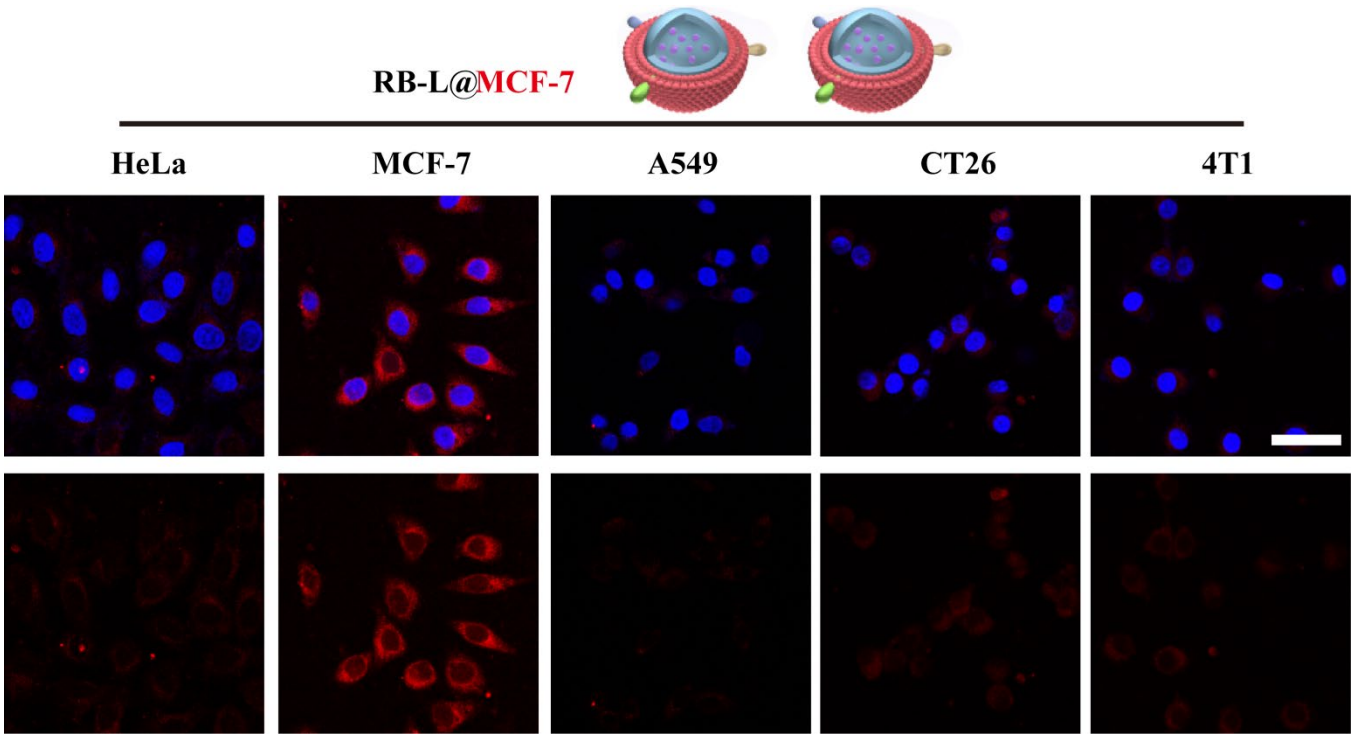

Figure S10. CLSM images of five cell lines including HeLa, MCF-7, A549, CT26 and 4T1 cells upon 4 h incubation with RB-L@MCF-7. The nuclei were stained with Hoechst (blue). Scale bar: 50 μm.

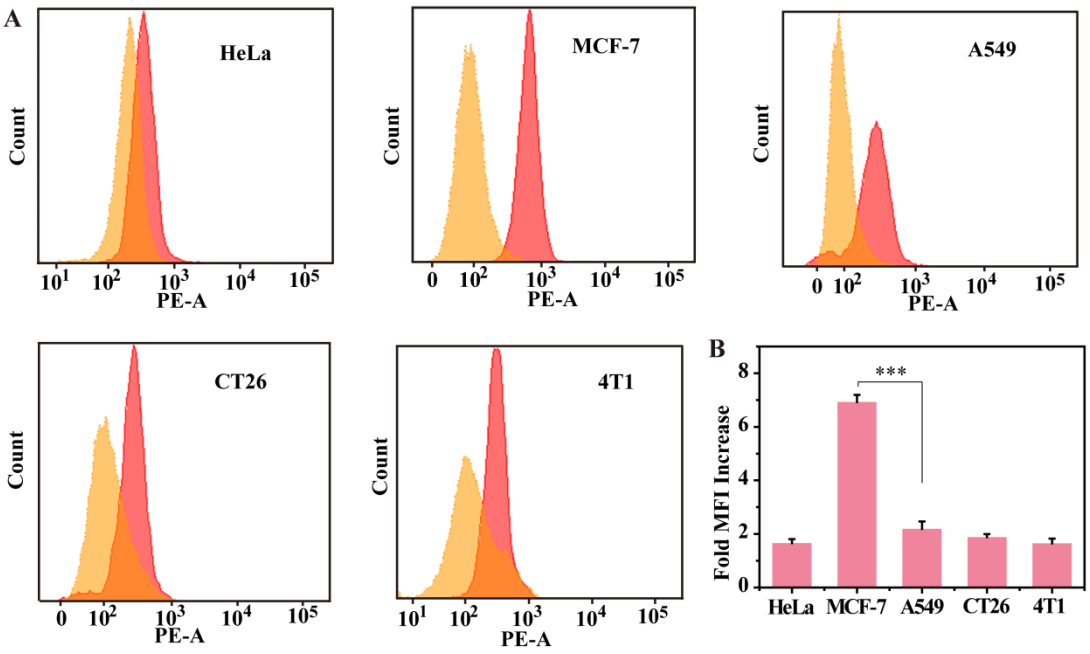

Figure S11. (A, B) Flow cytometry analysis of various cells incubated with RB-L@ MCF-7 for 4 h. Error bars were calculated on the basis of three independent experiments. Asterisks indicated significant differences (*P < 0.05, **P < 0.01, ***P < 0.001).

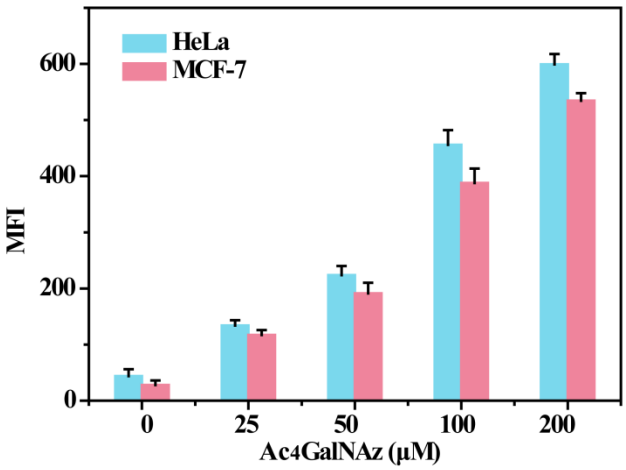

Figure S12. Flow cytometry analysis of HeLa and MCF-7 cells metabolically labeled with free Ac_4GalNAz for 12 h. The cells were subsequently labeled with DBCO-Cy5 and analyzed by flow cytometry. Error bars represent the standard deviation from three replicate experiments.

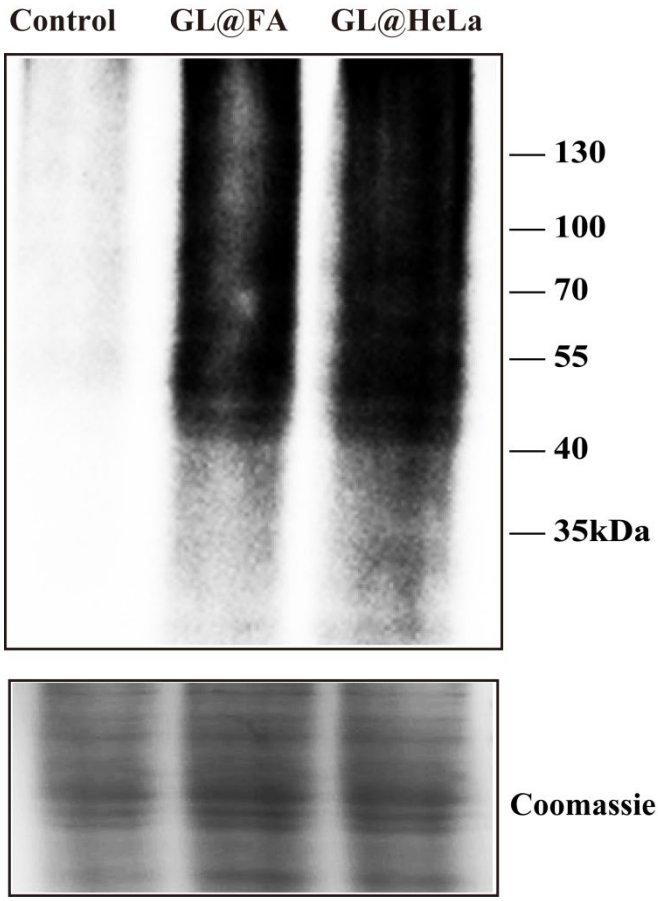

Figure S13. Western blot analysis of azide groups in glycoproteins of cells treated with GL@FA, GL@HeLa or PBS as control for 24 h. (50 μM, calculated based on Ac_4GalNAz). The coomassie stain shows the total amount of protein.

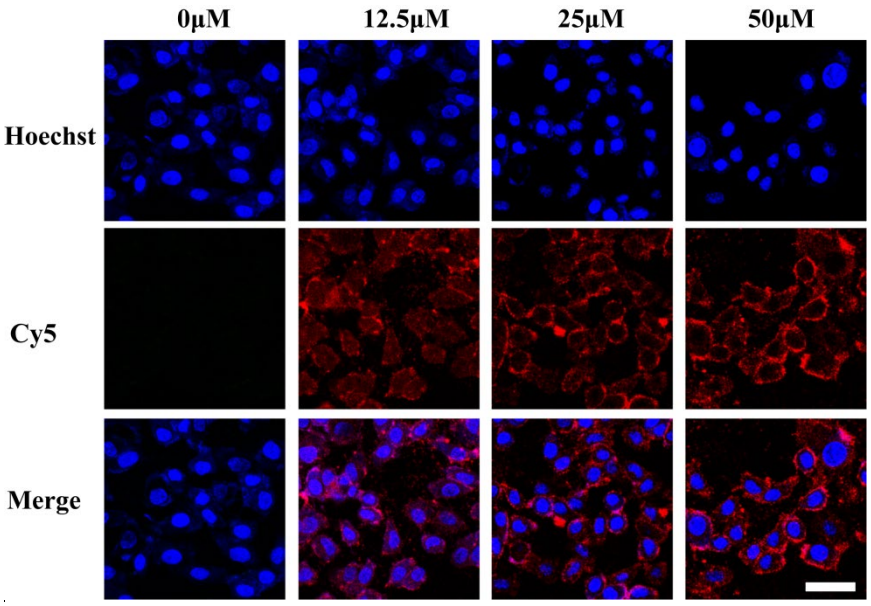

Figure S14. CLSM images of live HeLa cells treated with different concentrations of GL@HeLa for 24 h (calculated based on $Ac_4GalNAz$). The cells were subsequently labeled with DBCO-Cy5. The nuclei were visualized by staining with Hoechst 33342. Scale bar: 20 μm.

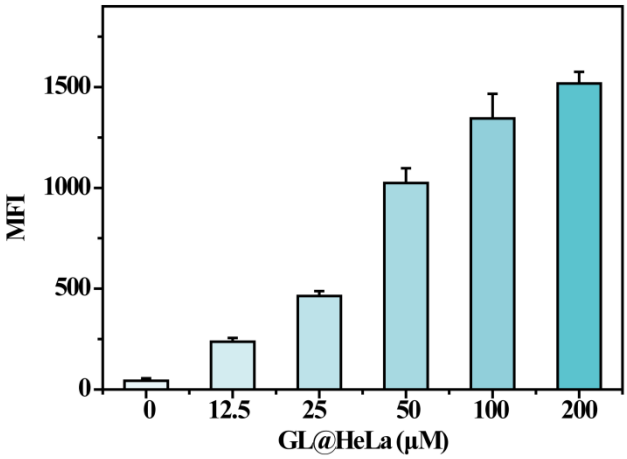

Figure S15. Flow cytometry analysis of HeLa cells treated with GL@HeLa at various concentrations for 24 h (calculated based on Ac_4GalNAz). The cells were subsequently labeled with DBCO-Cy5 and analyzed by flow cytometry. Error bars represent the standard deviation from three replicate experiments.

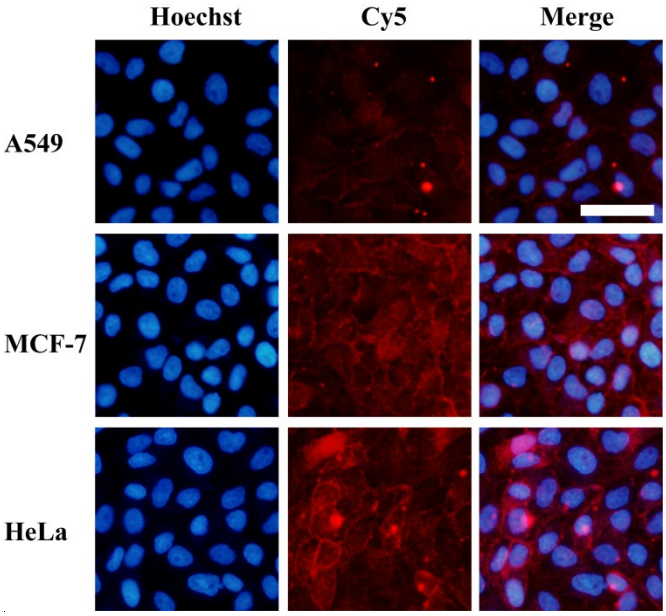

Figure S16. CLSM images of three cell lines including A549, MCF-7 and HeLa cells upon 24 h incubation with 50 μM GL@FA (calculated based on Ac_4GalNAz). The cells were subsequently labeled with DBCO-Cy5. The nuclei were visualized by staining with Hoechst 33342. Scale bars: 50 μm.

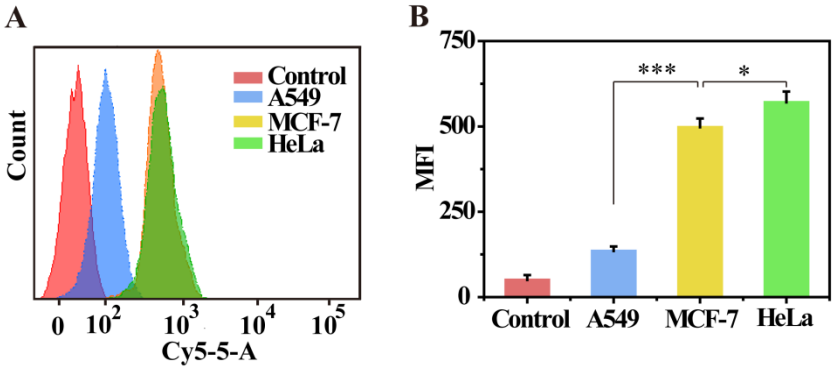

Figure S17. (A, B) Flow cytometry analysis of different cells incubated with 50 μM GL@FA (calculated based on Ac_4GalNAz) nanoparticles for 24 h. The cells were subsequently labeled with DBCO-Cy5 and analyzed by flow cytometry. Error bars represent the standard deviation from three replicate experiments. Asterisks indicated significant differences (*P < 0.05, **P < 0.01, ***P < 0.001).

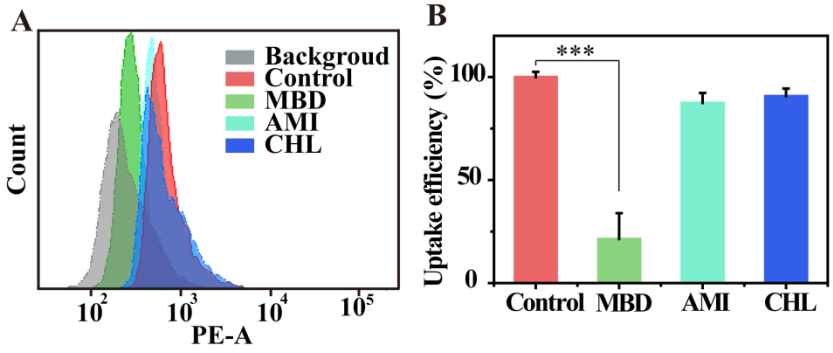

Figure S18. Endocytosis pathway of cancer cell membrane-camouflaged liposomes in HeLa cells. (A) Flow cytometry analysis of HeLa cells treated with RB-L@HeLa and different endocytosis pathway inhibitors. (B) Uptake efficiency of RB-L@HeLa by HeLa cells incubated with different inhibitors. Error bars were calculated on the basis of three independent experiments. Asterisks indicated significant differences (*P < 0.05, **P < 0.01, ***P < 0.001).

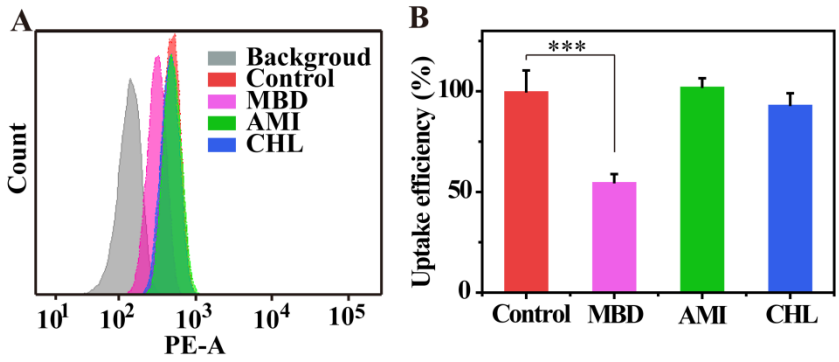

Figure S19. Endocytosis pathway of cancer cell membrane-camouflaged liposomes in MCF-7 cells. (A) Flow cytometry analysis of MCF-7 cells treated with RB-L@MCF-7 and different endocytosis pathway inhibitors. (B) Uptake efficiency of RB-L@ MCF-7 by MCF-7 cells incubated with different inhibitors. Error bars were calculated on the basis of three independent experiments. Asterisks indicated significant differences (*P < 0.05, **P < 0.01, ***P < 0.001).

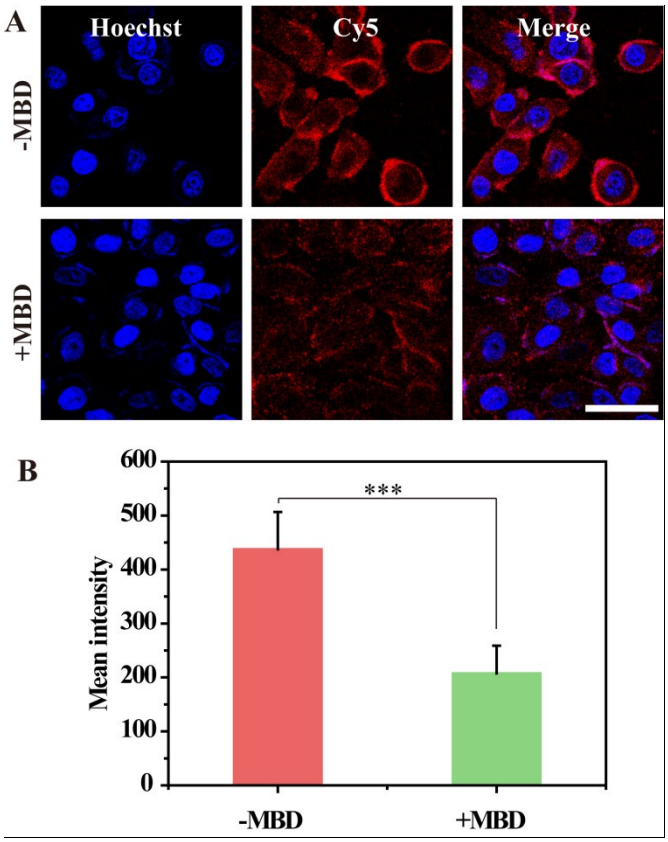

Figure S20. (A) CLSM images of HeLa cells incubation with 50 μM GL@HeLa in the presence or absence of 5 mM methyl-beta cyclodextrin (MBD). The nuclei were stained with Hoechst (blue). Then treated cells were fluorescently labeled by DBCO-Cy5. (B) Quantification of mean fluorescence intensity of confocal microscopy images using Nikon Eclipse Analysis software. Data were presented as mean intensity. (n = 10) Scale bars: 50 μm. Error bars were calculated on the basis of three independent experiments. Asterisks indicated significant differences (*P < 0.05, **P < 0.01, ***P < 0.001).

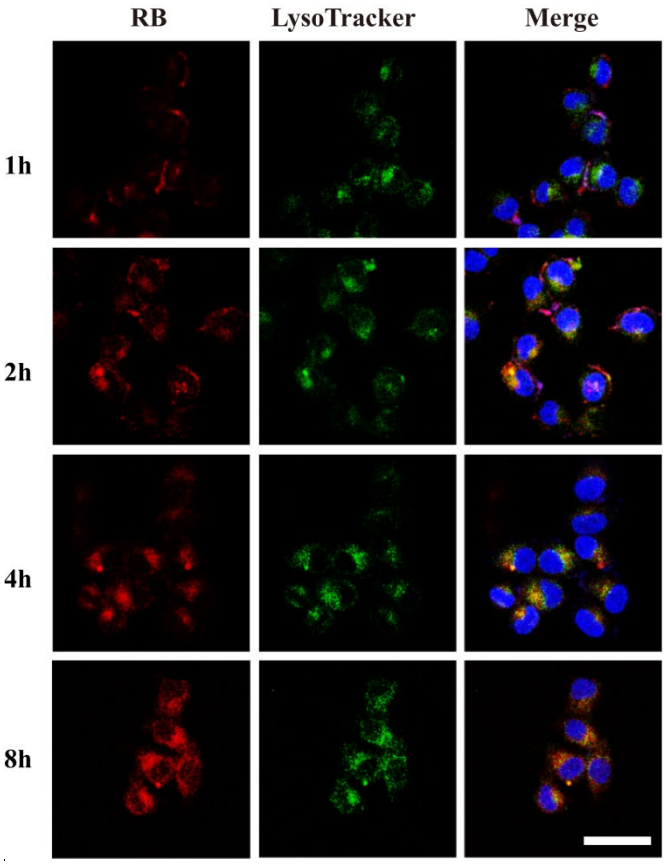

Figure S21. Time-dependent intracellular colocalization of RB-L@HeLa with lysome in HeLa cells. The nuclei were stained with Hoechst (blue). Scale bars: 50 μm.

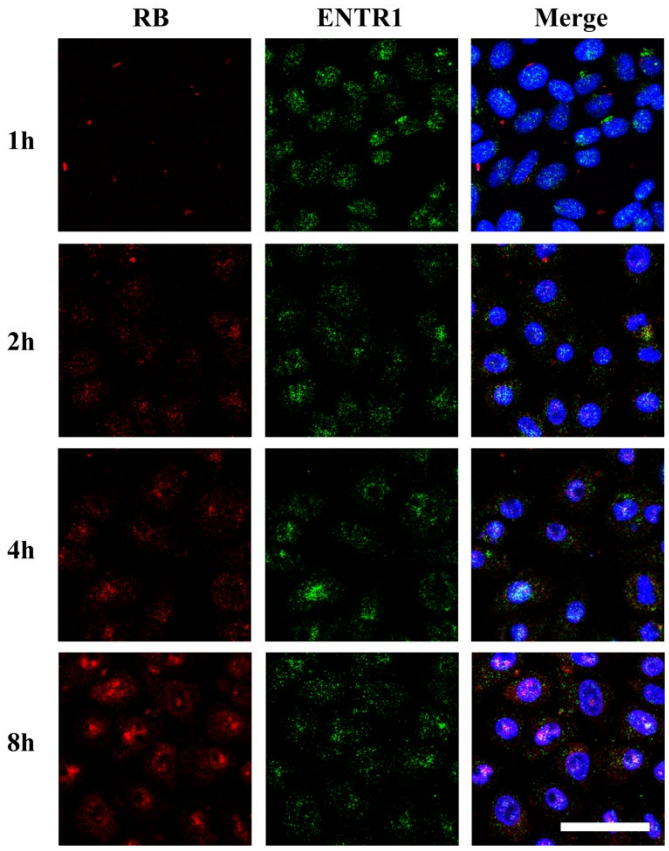

Figure S22. Time-dependent intracellular colocalization of RB-L@HeLa with endosome in HeLa cells. The endosome was stained by endosome associated trafficking regulator 1 (ENTR 1) antibody (green). The ENTR 1 was an endosome associated protein (8). The liposomes were tracked with RB (red) and the nuclei were stained with Hoechst (blue). Scale bars: 50 μm.

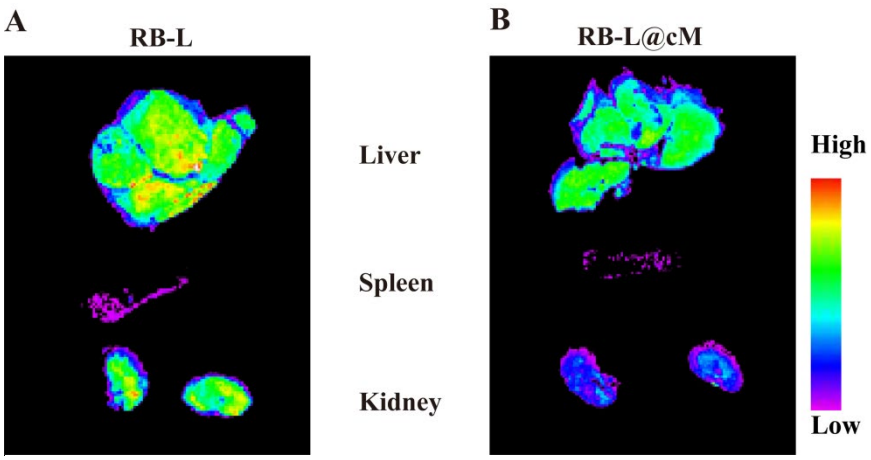

Figure S23. Ex vivo imaging of organs including liver, spleen, kidney harvested from healthy mice treated with RB-L and RB-L@cM for 12 h.

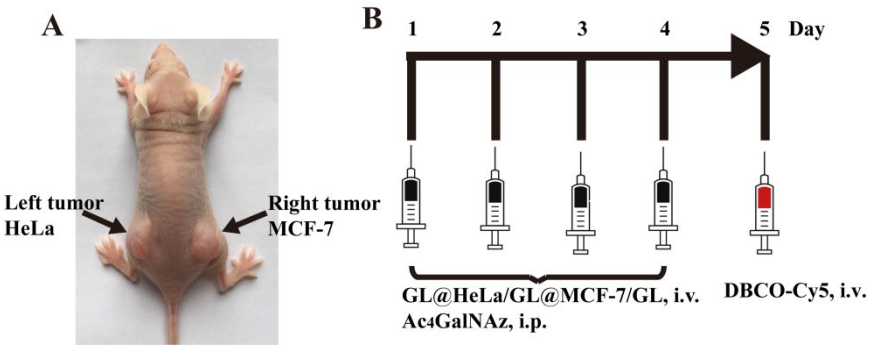

Figure S24. Time course of in vivo labeling study in athymic nude mice bearing two kinds of tumors.

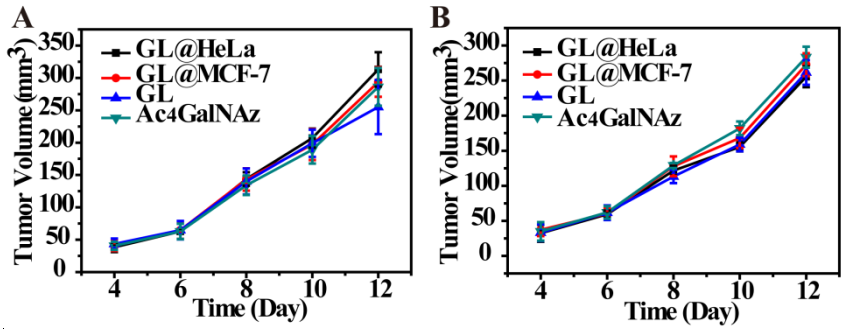

Figure S25. Growth rate of HeLa and MCF-7 tumors in Balb/c nude mice. (A) The HeLa tumors in mice injected with GL@HeLa, GL@MCF-7, GL and $Ac_4GalNAz$. (B) The MCF-7 tumors in mice injected with GL@HeLa, GL@MCF-7, GL and $Ac_4GalNAz$.

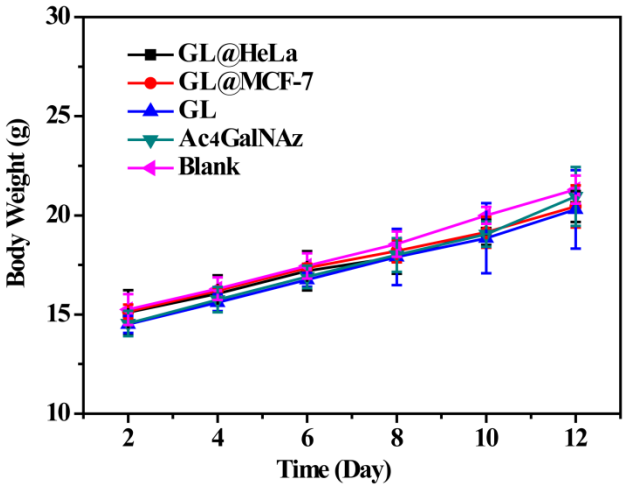

Figure S26. Body weight of mice administrated with GL@HeLa, GL@MCF-7, GL, Ac_4GalNAz and PBS as Blank.

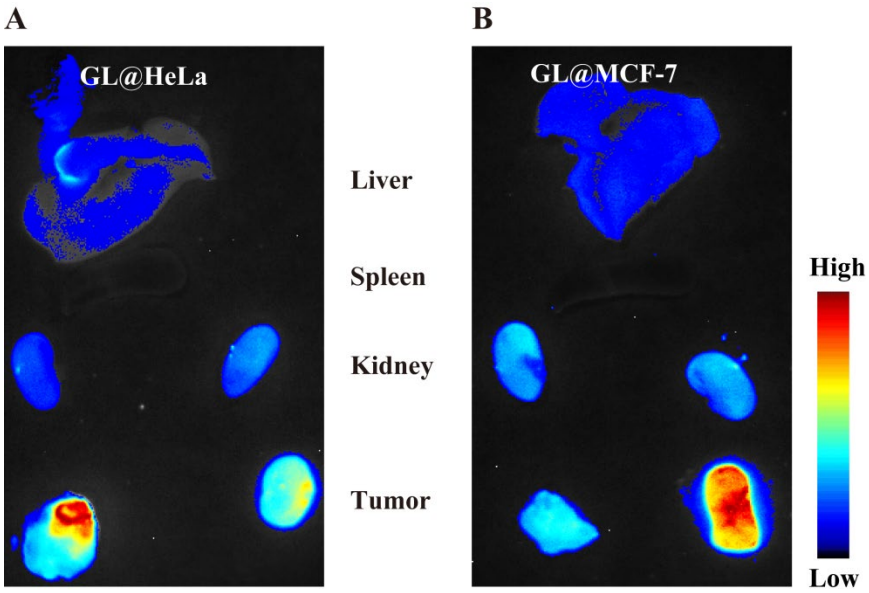

Figure S27. Ex vivo imaging of tumors and organs including liver, spleen, kidney harvested from mice treated with GL@HeLa and GL@MCF-7.

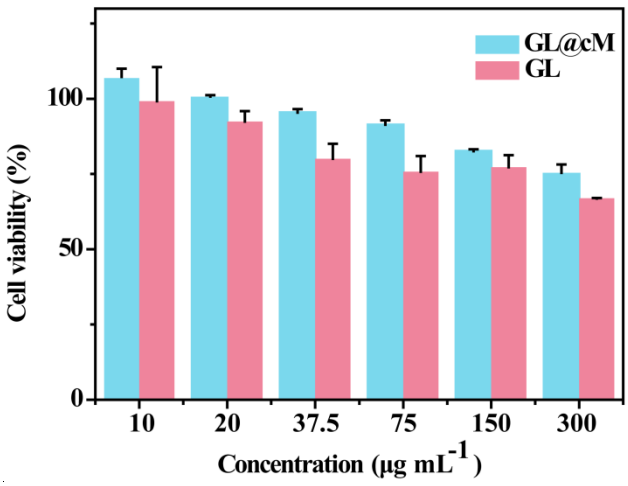

Figure S28. In vitro biocompatibility of GL@cM and GL. Cell viability of HeLa cells treated with different concentration of nanoparticles for 24 h. (300 μg mL^{-1} GL@cM equal to 126 μM $Ac_4GalNAz$)

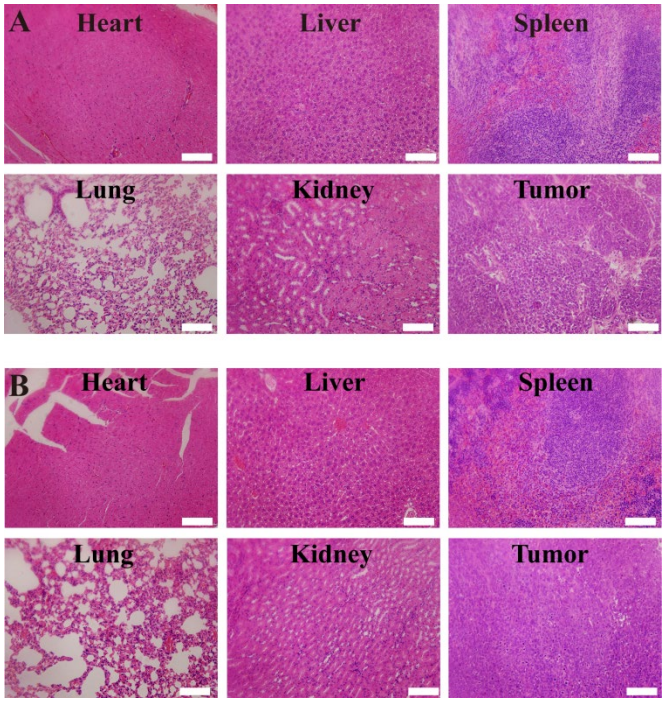

Figure S29. Histological (H&E) images of the major organs and tumors after treatment showed no evident systemic toxicity of the biomimetic GL@HeLa nanoparticles. (A) PBS group. (B) GL@HeLa nanoparticles group. Scale bar: 100 μm.

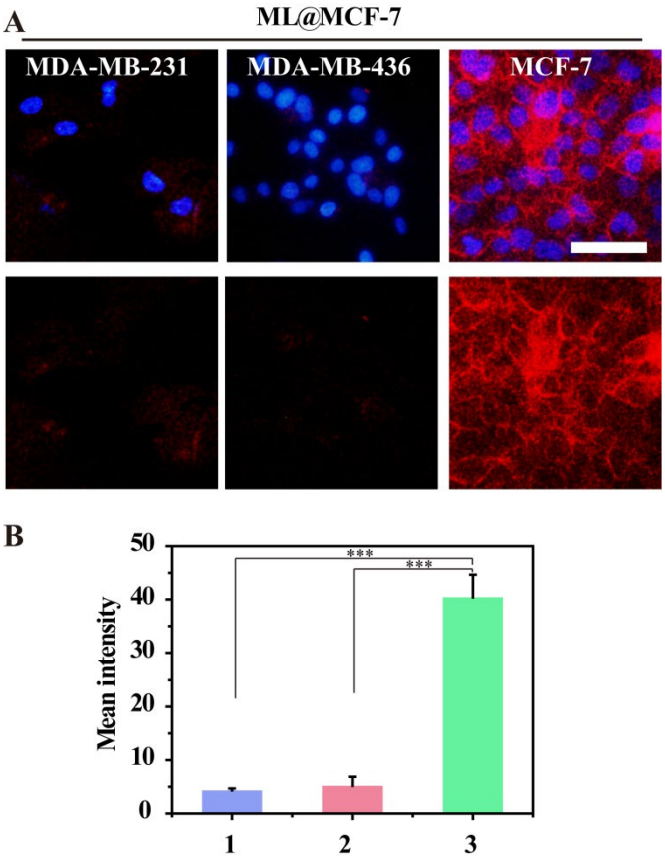

Figure S30. (A) Fluorescence micrographs of different breast cancer subtypes including TNBC cells treated with ML@MCF-7. Then treated cells were labeled by DBCO-Cy5 (red).The nuclei were stained with Hoechst (blue). Scale bars: 50 μm. (B) Quantification of fluorescence intensity of images from (A) by ImageJ software. Data were presented as mean intensity. (n = 10) Asterisks indicated significant differences (*P < 0.05, **P < 0.01, ***P < 0.001).

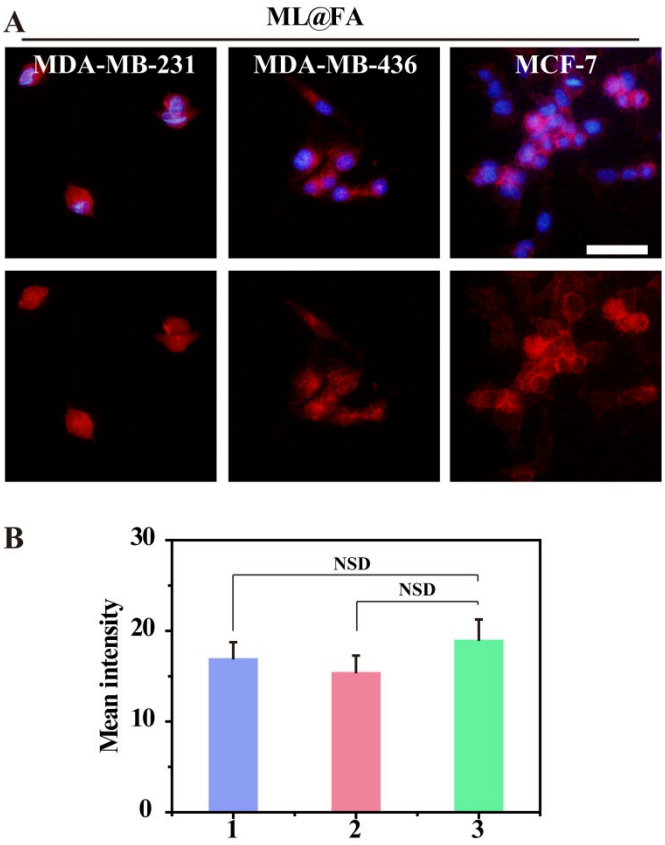

Figure S31. (A) Fluorescence micrographs of different breast cancer subtypes including TNBC cells treated with ML@FA. Then treated cells were labeled by DBCO-Cy5 (red). The nuclei were stained with Hoechst (blue). Scale bars: 50 μm. (B) Quantification of fluorescence intensity of images from (A) by ImageJ software. Data were presented as mean intensity. (n = 10) Asterisks indicated significant differences (NSD: no significant difference, *P < 0.05, **P < 0.01, ***P < 0.001).

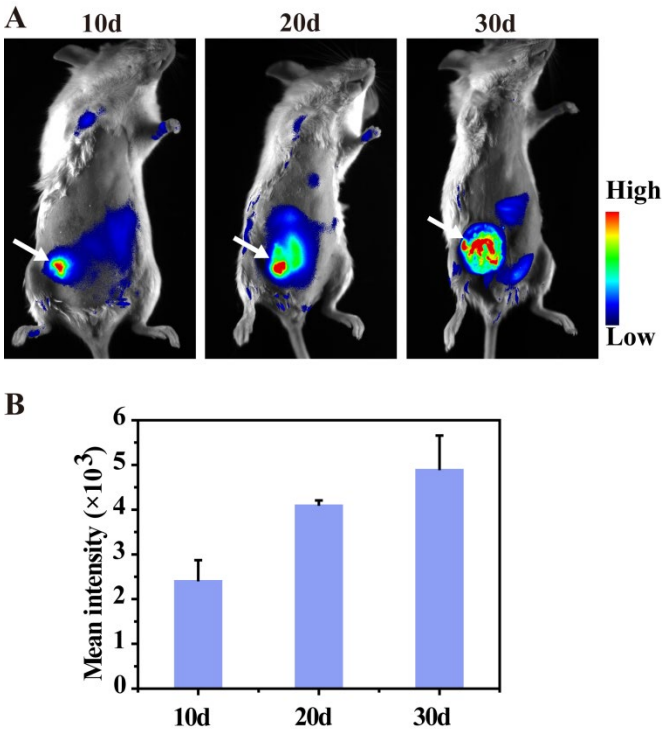

Figure S32. Probing the dynamic changes of mucin-type glycans during tumor growth. (A) Representative fluorescence images of tumor-associated glycans in mouse models. After tumor growth for 6, 16, and 26 days, GL@4T1 was injected into the mice for another 4 days, followed by administration with DBCO-Cy5 for whole-body fluorescence images. (B) Quantification of the fluorescence signal. Error bars were calculated on the basis of three independent experiments.

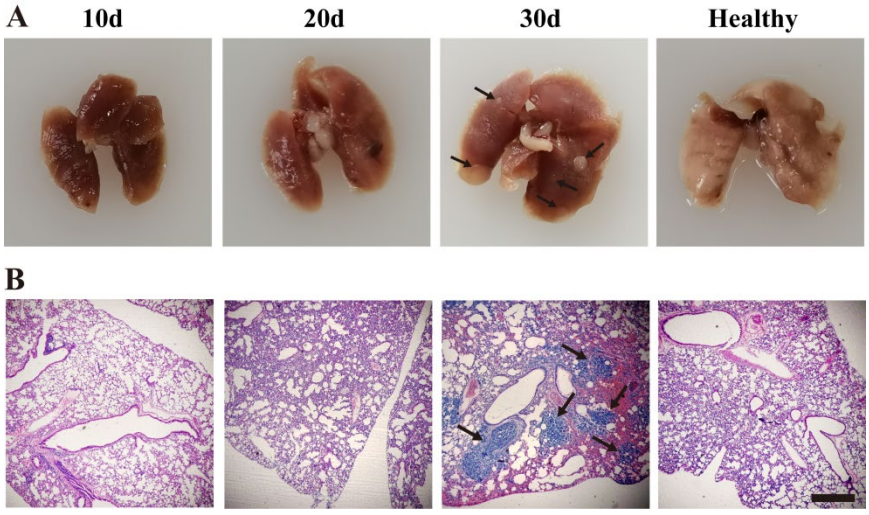

Figure S33. (A) Collected lung tissues and (B) H&E staining of the lung tissues at different time points. The black arrows indicated the metastatic nodules. Scale bar: 500 μm.

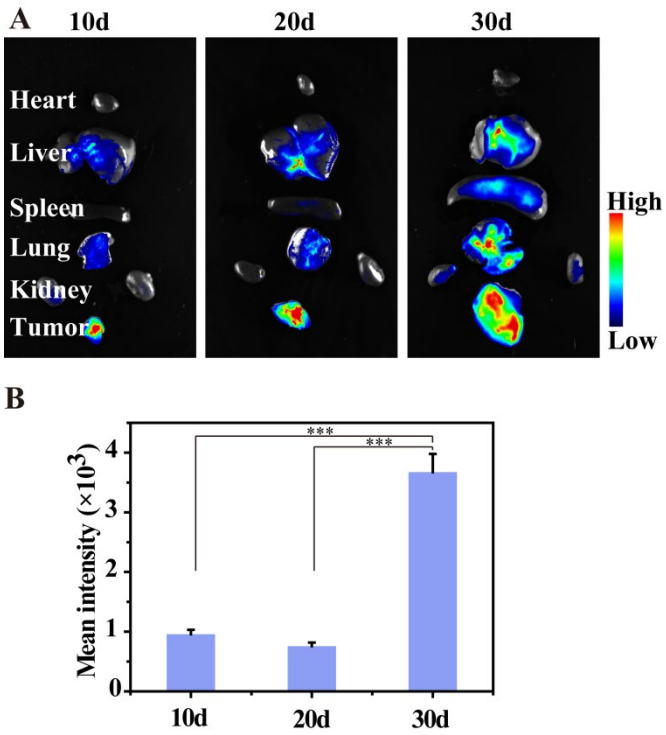

Figure S34. (A) Ex vivo fluorescence imaging of tissues harvested from mice at different time points. (B) Quantification of the fluorescence signal. Error bars were calculated on the basis of three independent experiments. Asterisks indicated significant differences (*P < 0.05, **P < 0.01, ***P < 0.001).

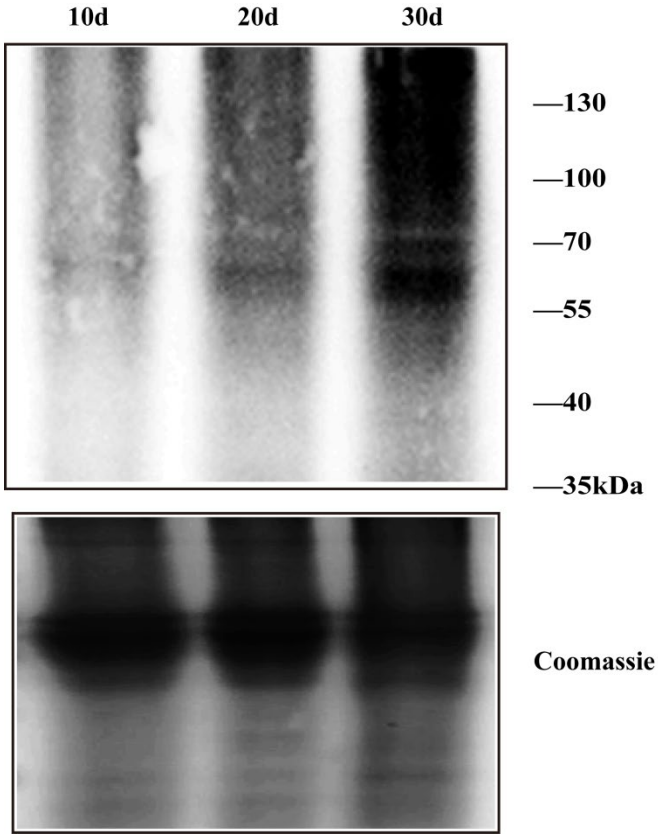

Figure S35. Western blot analysis of tumor lysates isolated on day 10, 20, and 30 from mice implanted with 4T1 tumors for 6, 16, and 26 days, followed by a 4-day administration of GL@4T1. The coomassie stain shows the total amount of protein.

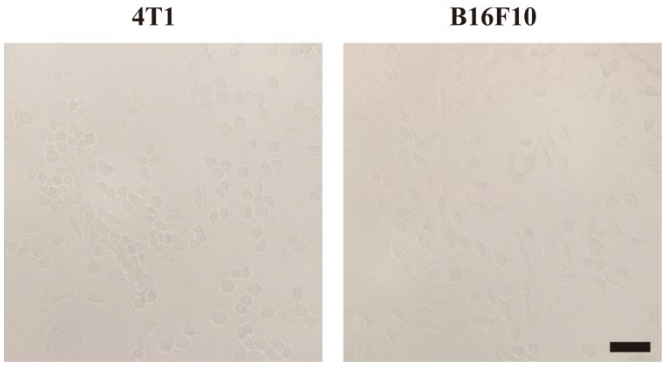

Figure S36. The optical microscope photographs showed the cancer cells extracted from 4T1 and B16F10 tumor tissues. Scale bar: 50 μm.

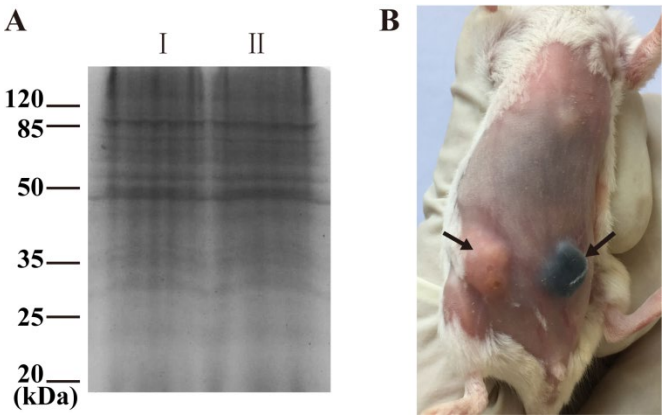

Figure S37. Protein profiles in the (I) cM from extracted 4T1 cells and (II) GL@4T1 characterized by SDS-PAGE. (B) Immune competent balb/c mice implanted with orthotopic tumors (4T1 tumors on the left and B16F10 tumors on the right).

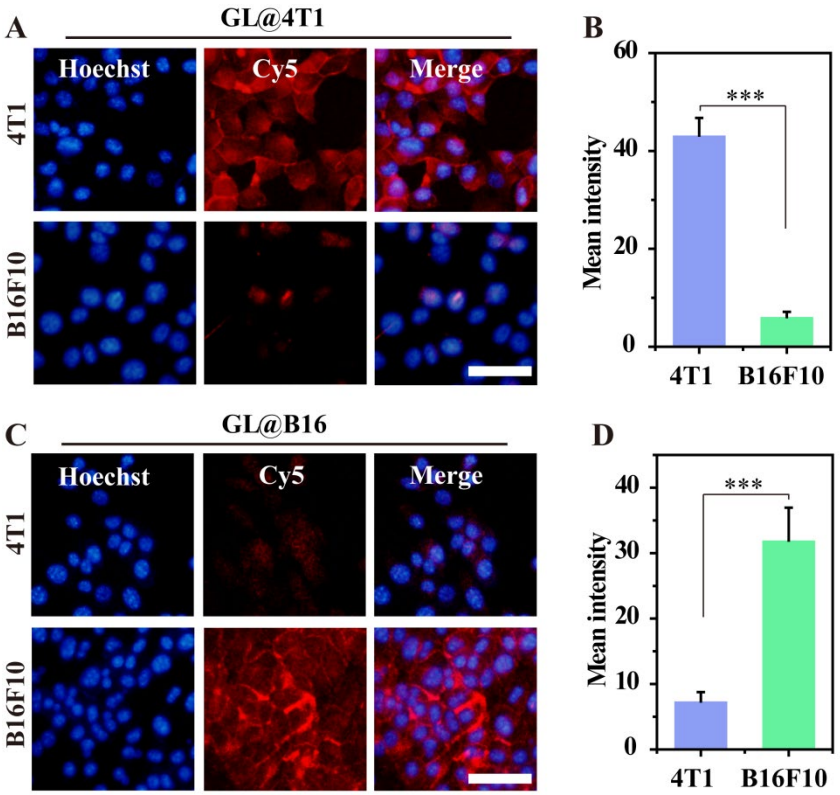

Figure S38. (A, C) Fluorescence micrographs of different cancer cells treated with GL@4T1 or GL@B16. The cell membranes derived from tumor tissues. Then treated cells were labeled by DBCO-Cy5 (red). The nuclei were stained with Hoechst (blue). Scale bars: 50 μm. (B, D) Quantification of fluorescence intensity of images from (A, C) by Image J software. Data were presented as mean intensity. (n = 10) Asterisks indicated significant differences (*P < 0.05, **P < 0.01, ***P < 0.001).

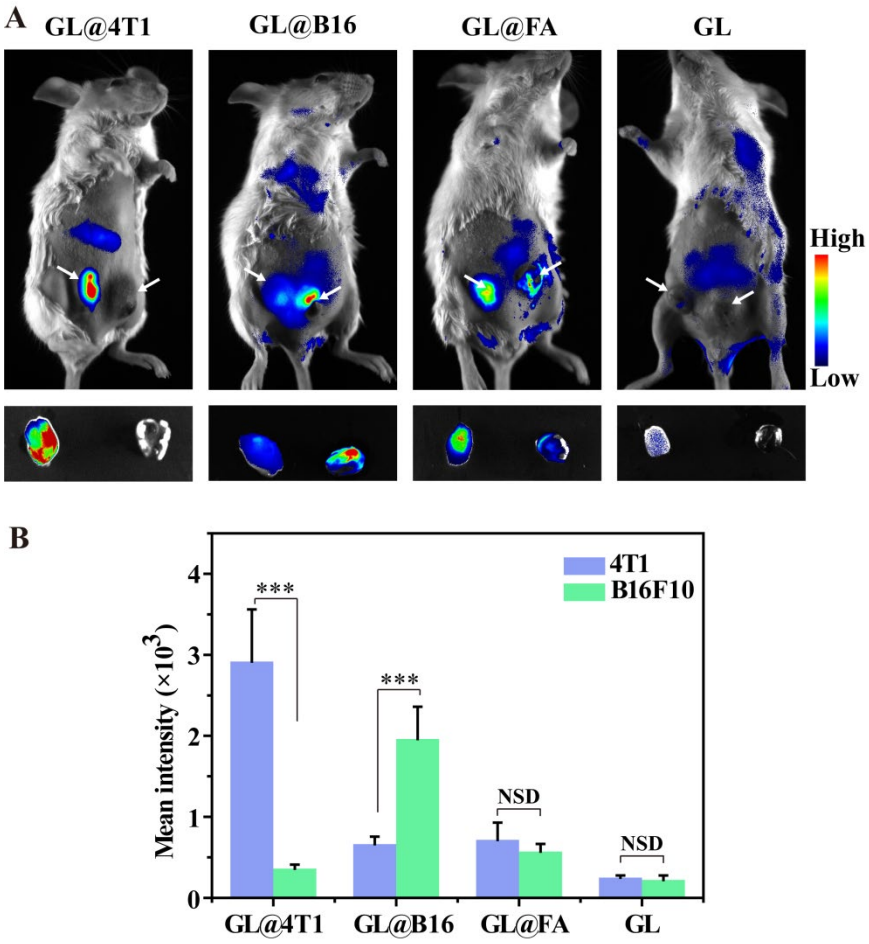

Figure S39. In vivo selective fluorescence imaging of tumor-associated glycans using GL coated with tumor tissues-derived cell membranes. (A) Whole-body fluorescence images of tumor-bearing mice injected with GL@4T1 (60 mg kg^{-1}), GL@B16 (60 mg kg^{-1}), GL@FA (60 mg kg^{-1}), and GL (60 mg kg^{-1}) for 4 days. On fifth day, DBCO-Cy5 was administrated into the mice. (B) Quantification of the fluorescence signal. Error bars were calculated on the basis of three independent experiments. Asterisks indicated significant differences (NSD: no significant difference, *P < 0.05, **P < 0.01, ***P < 0.001).

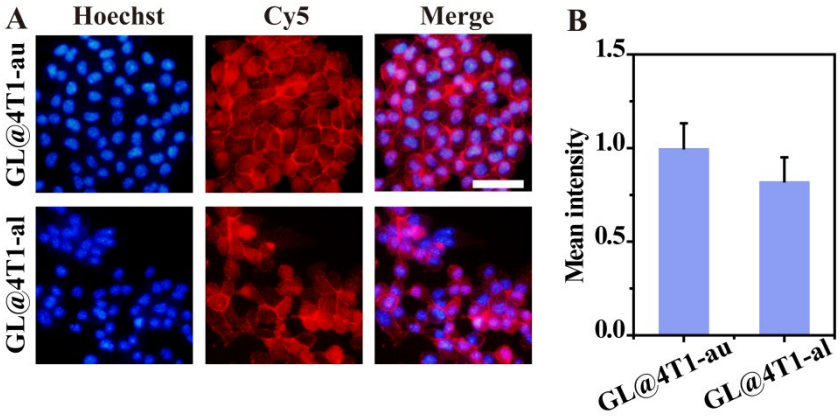

Figure S40 . (A) Fluorescence micrographs of cells incubated with GL@4T1-au and GL@4T1-al. Then treated cells were labeled by DBCO-Cy5 (red). The nuclei were stained with Hoechst (blue). Scale bars: 50 μm. (B) Quantification of fluorescence intensity of images from (A) by ImageJ software. Data were presented as mean intensity. (n = 10) Asterisks indicated significant differences (*P < 0.05, **P < 0.01, ***P < 0.001).

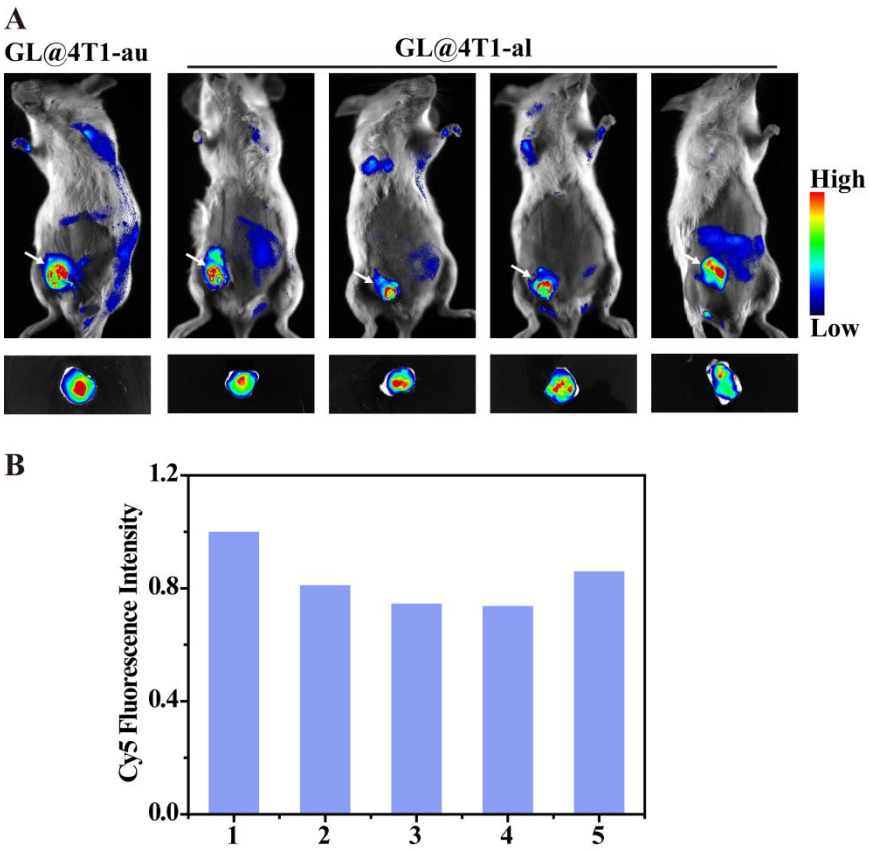

Figure S41. In vivo selective tumor glycans imaging of mice using GL coated with different tumor tissues-derived cell membranes. (A) Whole-body fluorescence images of tumor-bearing mice injected with GL@4T1-au and GL@4T1-al (60 mg kg^{-1}) for 4 days. On fifth day, DBCO-Cy5 was administrated into the mice. (B) Quantification of the fluorescence signal in (A).

Table S1. The loading capacity of different cancer cell membrane camouflaged liposomes quantified by HPLC analysis

Nanoparticles	Azidosugar	Loading capacity (%)
GL	Ac_4GalNAz	20.8
GL@FA	Ac_4GalNAz	23.5
GL@HeLa	Ac_4GalNAz	18.1
GL@MCF-7	Ac_4GalNAz	16.7
GL@B16	Ac_4GalNAz	17.4
GL@4T1	Ac_4GalNAz	15.4
GL@4T1-au	Ac_4GalNAz	14.8
GL@4T1-al	Ac_4GalNAz	15.9
ML	Ac_4ManNAz	23.2
ML@FA	Ac_4ManNAz	21.1
ML@MDA-436	Ac_4ManNAz	19.6
ML@MDA-231	Ac_4ManNAz	18.4
ML@MCF-7	Ac_4ManNAz	16.3

References:

1. J.Y. Zhu*, et al.*, Preferential Cancer Cell Self-Recognition and Tumor Self-Targeting by Coating Nanoparticles with Homotypic Cancer Cell Membranes. *Nano Lett* **16**:5895-5901 (2016).
2. R. Xie*, et al.*, Targeted imaging and proteomic analysis of tumor-associated glycans in living animals. *Angew Chem Int Ed* **53**:14082-14086 (2014).
3. L. Du, H. Qin, T. Ma, T. Zhang, D. Xing, In Vivo Imaging-Guided Photothermal/Photoacoustic Synergistic Therapy with Bioorthogonal Metabolic Glycoengineering-Activated Tumor Targeting Nanoparticles. *ACS Nano* **11**:8930-8943 (2017).
4. G. Cheng*, et al.*, Self-Assembly of Extracellular Vesicle-like Metal-Organic Framework Nanoparticles for Protection and Intracellular Delivery of Biofunctional Proteins. *J Am Chem Soc* **140**:7282-7291 (2018).
5. Y. Sun*, et al.*, Mechanistic Investigation and Multiplexing of Liposome-Assisted Metabolic Glycan Labeling. *J Am Chem Soc* **140**:3592-3602 (2018).
6. H. Wang*, et al.*, Targeted Ultrasound-Assisted Cancer-Selective Chemical Labeling and Subsequent Cancer Imaging using Click Chemistry. *Angew Chem Int Ed* **55**:5452-5456 (2016).
7. L. Xiao, J.V. McCann, A.C. Dudley, Isolation and Culture Expansion of Tumor-specific Endothelial Cells. *JoVE-J Vis Exp*: e53072 (2015).
8. S. Sharma*, et al.*, Apoptotic signalling targets the post-endocytic sorting machinery of the death receptor Fas/CD95. *Nat Commun* **10**:3105 (2019).